An artificial intelligence approach to design periodic nonlinear oscillator chains under external excitation with stable damped solitons

Arthur Barbosa, Joao Pedro Sena, Najib Kacem, Noureddine Bouhaddi

An artificial intelligence approach to design periodic nonlinear oscillator chains under external excitation with stable damped solitons

A. Barbosa[a,*], J.P. Sena[b], N. Kacem[a], N. Bouhaddi[a]

[a] *University of Franche-Comté, CNRS, FEMTO-ST Institute, Department of Applied Mechanics, 26 Rue de l'Épitaphe, Besançon, 25000, Franche-Comté, France*
[b] *Federal University of Uberlândia, Department of Mechanics, 1M - Santa Mônica, Uberlândia, 38408-100, Minas Gerais, Brazil*

Abstract

In this paper, an artificial intelligence approach is developped to create a metamodel of damped solitons in periodic nonlinear oscillator chains under external excitation. Unlike resonators subjected to parametric excitation, chains subjected exclusively to external excitation do not have known analytical solutions for Intrinsic Localized Modes (ILMs) when damping is pondered. The proposed metamodel is a quick design tool of nonlinear damped periodic structures describing effectively the behavior of solitonic solutions, demonstrating a computational cost considerably lower than that of the Newton method. The results of this work highlight the potential of ANN regression models in the description of physical phenomena represented by the Nonlinear Schrödinger Equation when damping is considered.

Keywords: Artificial Neural Networks, Damped stationary solitons,

*Corresponding author
Email addresses: arthur.barbosa@femto-st.fr (A. Barbosa), joaopedrosena@ufu.br (J.P. Sena), najib.kacem@femto-st.fr (N. Kacem), noureddine.bouhaddi@femto-st.fr (N. Bouhaddi)

1. Introduction and motivation

The Nonlinear Schrödinger equation (NLSE) plays a fundamental role in describing a series of physical phenomena, from the dynamics of micro-mechanical systems [1] to explaining nonlinear phenomena involving plasma physics [2]. Recent research examples apply the NLSE in several fields such as biology [3], optics [4], photonics [5], and metamaterials [6], highlighting the importance of seeking solutions to the solitonic problem of the NLSE.

Unlike other areas of study, damping plays a fundamental role in describing mechanical systems, adding complexity to the generation and control of nonlinear waves. Given this scenario, the theoretical and experimental reproduction of the NLSE in mechanical contexts is usually accomplished through chains of damped nonlinear oscillators subjected to external, parametric, or both excitations [7] and the reported applications are diverse, from modal analysis [8] to detecting masses in microcantilevers [9].

Due to the presence of damping, the search for closed-form solutions becomes a complex and often infeasible task for systems described by the NLSE. Under these circumstances, researchers have applied numerical strategies to search for stable solutions, and such methodologies are well-documented in the literature [10, 11, 12]. However, the computational efforts involved in such works are often high. An example of this issue is the use of the Newton method to delimit parameters that guarantee the existence of damped solitons [13].

The use of Artificial Neural Networks (ANN) regression models as meta-

models to solve complex problems associated with high computational cost has followed the rapid computing power growth. To illustrate this statement, we can mention the use of this strategy in the analysis of conservation laws from differential equations [17] and evolutions of nonlinear problems [15].

The massive interconnectivity between neurons and the ability to be trained using backpropagation are characteristics that allow the utilization of ANN to overcome challenges, such as the search for NLSE solutions [14, 16]. The development of metamodels associated with solitonic equations proved to be a promising strategy. Despite the advances in the use of artificial intelligence in describing solitonic phenomena [18, 19], until now, metamodels capable of describing damped solitons subjected to external excitation have not yet been reported in the literature.

To our knowledge, the exploration of localized vibrations in coupled resonators is an additional motivation behind this work. With the analysis of Intrinsic Localized Modes (ILM) presenting as a potential field for several mechanical engineering applications, including those detailed in studies such as [20, 21, 22, 23, 24], it is important to further improve our understanding of these modes, particularly in damped structures.

In this scenario, the present work aims to apply Neural Networks techniques for the creation of a metamodel of stationary solitons that describe the amplitude of vibration of damped oscillator chains subjected to an external force. Unlike resonators subjected to parametric excitation, chains subjected exclusively by external excitation do not have known analytical solutions for ILMs when damping is considered, ratifying the advantage that a metamodel could add to applications that use such systems.

The obtained metamodel proved to be effective in describing the behavior of damped stationary solitons when an external excitation is considered within a parameter region. The computational cost of the metamodel, compared with the Newton's method, demonstrated to be considerably inferior, confirming the advantages of this approach without significant loss of accuracy of the predicted solutions.

The rest of the paper is arranged as follows: Section 2 presents the state-of-the-art of stationary solitons in oscillator chains, where a description about the context of the research motivation is made. An approach for searching stationary solutions of the NLSE is presented in Section 3. The development of the metamodel and region of accuracy, in Section 4 and Section 5, respectively. Finally, the conclusion and possible future directions are given in Section 6.

2. State-of-the-art of stationary solitons in oscillator chains with cubic nonlinearity

The mechanical configuration depicted in Fig 1 is a generalized version of the system under investigation in this study. It comprises a chain of nonlinear oscillators subjected to different types of damping. The structure also considers two types of excitation: external and parametric. The mathematical description of this system was provided by [7] and is expressed through

the following equation:

$$
\begin{aligned}
&M\ddot{X}_n + C\dot{X}_n + KX_n + \Xi X_n^3 + \Delta X_n^2 \dot{X}_n \\
&-K_d\left(X_{n+1} - 2X_n + X_{n-1}\right) \\
&+\Psi\left[\left(X_n - X_{n+1}\right)^3 + \left(X_n - X_{n-1}\right)^3\right] \\
&+\Phi\left[\left(X_n - X_{n+1}\right)^5 + \left(X_n - X_{n-1}\right)^5\right] \\
&+\Lambda\left[\left(X_n - X_{n+1}\right)^2\left(\dot{X}_n - \dot{X}_{n+1}\right)\right] \\
&+\Lambda\left[\left(X_n - X_{n-1}\right)^2\left(\dot{X}_n - \dot{X}_{n-1}\right)\right] \\
&= H\cos\left(\omega_e t\right) - G\cos\left(\omega_p t\right) X_n.
\end{aligned}
\tag{1}
$$

The displacement of the n^{th} oscillator from its equilibrium position at the time t is given by the variable X_n, where n ranges from 0 to $(N+1)$ with known boundary conditions (such as $X_0 = X_{N+1} = 0$). Each oscillator is excited by both a parametric excitation with frequency ω_p and an external excitation with frequency ω_e. The parametric and external excitation amplitudes are represented by G and H, respectively. The system's parameters include effective mass M, effective spring constant K, nonlinear stiffness Ξ, coupling Duffing parameter Ψ, nonlinear quintic coupling parameter Φ, linear damping C, coupling spring constant K_d, Duffing-Van Der Pol damping Δ, and nonlinear dissipative coupling Λ.

Since the solution's derivation of Equation (1) is beyond the scope of this work, its development will not be shown in this paper. Following the procedure adopted in [7], it is possible to express the behavior of the system shown in Fig 1 through the method of multiple scales, where the cancellation of secular terms leads to the emergence of an expression that describes the

amplitude of the oscillators by a solitonic equation:

$$i\frac{\partial\psi}{\partial T} = -\frac{\partial^2\psi}{\partial x^2} + (1 - i\gamma)\psi - (2 + i\eta)|\psi|^2\psi + g\bar{\psi} - h. \tag{2}$$

The Equation (2) is a generic form of the one-dimensional mechanical NLSE with cubic nonlinearity where γ is related to linear damping, η is related to nonlinear damping, g is related to the amplitude of parametric excitation, h is related to the amplitude of external force, ψ is related to the amplitude of the oscillators, x is the normalized spatial variable, T is the normalized time variable, and $\bar{\psi}$ is the conjugate of ψ.

Other studies have adopted similar methodologies and have documented the connection between chains of nonlinear oscillators and solitons in a variety of systems such as coupled pendulums [25], circular structures [26] and linear architecture coupled oscillators [27]. Despite the extensive investigations in this field, an analytical solution for Equation (2) remains unknown. Nevertheless, stationary solutions for certain specific cases are available in the literature (see Table 1).

The cases D, E, F, and G are of fundamental interest for macro-mechanical systems since the presence of damping should be taken into consideration in more general models, particularly for the linear damping. Considering that external excitation can be found in various applications, whether in the form of base acceleration or driving forces [28], case E will be the focus of this work. The particularization of Equation (2) for this case leads us to the expression:

$$i\frac{\partial\psi}{\partial T} = -\frac{\partial^2\psi}{\partial x^2} + (1 - i\gamma)\psi - 2|\psi|^2\psi - h, \tag{3}$$

Table 1: Stationary solutions for different configurations of Equation (2) found in the literature.

Case	Damping	Excitation	Solution
A	$\gamma = 0$, $\eta = 0$	$g = 0$, $h = 0$	Analytical [24]
B	$\gamma = 0$, $\eta = 0$	$g = 0$, $h > 0$	Analytical [13]
C	$\gamma = 0$, $\eta = 0$	$g > 0$, $h = 0$	Analytical [1]
D	$\gamma > 0$, $\eta = 0$	$g > 0$, $h = 0$	Analytical [1]
E	$\gamma > 0$, $\eta = 0$	$g = 0$, $h > 0$	Numerical [13]
F	$\gamma > 0$, $\eta = 0$	$g > 0$, $h > 0$	Numerical [7]
G	$\gamma > 0$, $\eta > 0$	$g > 0$, $h = 0$	Approximate analytical [1]

which will be investigated in this work.

Other configurations regarding the nonlinear factor are found in different applications, such as in [29], where the authors derived a NLSE with quintic nonlinearity in the description of solitary waves in the helicoidal Peyrard-Bishop-Dauxois model of deoxyribonucleic acid (DNA).

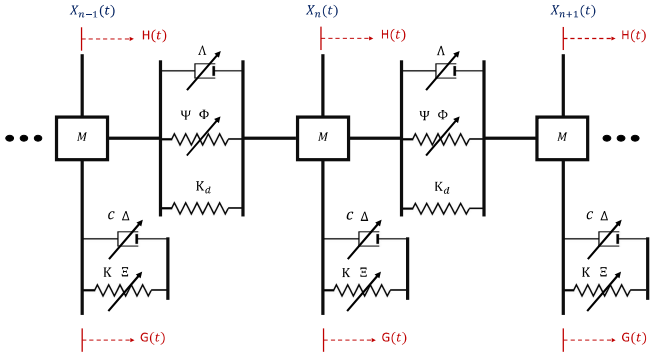

Figure 1: Equivalent system representing chains of nonlinear coupled oscillators subject to external and parametric excitation.

3. Search for stationary solutions for case E

3.1. Numerical solutions by the Newton's method

Equation (3) has three stationary solutions $\left(\frac{\partial\psi}{\partial T}=0\right)$ [13, 30]: dark solitons ψ_-, bright solitons ψ_+, and flat ones. Therefore, for a given pair of h and γ, the investigation of stationary solitons must necessarily use the numerical continuation strategy. Disregarding the flat solutions, stationary solitons described by the equation

$$\frac{\partial^2\psi}{\partial x^2}+(i\gamma-1)\psi-2|\psi|^2\psi+h=0 \tag{4}$$

have two analytical forms for the non-damped case ($\gamma = 0$) [13]:

$$\psi_{\pm}(x) = \psi_0 \left(1 + \frac{2\sinh^2\alpha}{1 \pm \cosh\alpha\cosh(Ax)}\right), \tag{5}$$

where

$$h = \frac{\sqrt{2}\cosh^2\alpha}{\left(1+2\cosh^2\alpha\right)^{3/2}}, \qquad \psi_0 = \frac{1}{\sqrt{2\left(1+2\cosh^2\alpha\right)}}, \tag{6}$$

$$A = 2\psi_0 \sinh\alpha.$$

The strategy employed by [13] has proven to be effective, where, by the continuous analog of the Newton method (also known as the variable iteration step Newton method), the authors succeeded in delimiting an area of existence and stability of numerical solutions for damped cases.

According to [13], for case E, only dark solitons (ψ_-) can exhibit temporal stability. Consequently, from a physical point of view, chains of nonlinear oscillators could not have localized vibration modes described by ψ_+. Due to this fact, the solitons analyzed in this paper are based exclusively in ψ_-, without loss of generality in the methodology.

The initial stage of the numerical approach involves the discretization of Equation (4) where the following operator is defined:

$$F(\Psi) = 0, \tag{7}$$

for $\Psi = (\psi_0, \psi_1, \ldots, \psi_{N+1})$, $\psi_n = \psi(x_n), x_n = -\frac{L}{2} + n\Delta x$, $\Delta x = \frac{L}{N+1}$ and $F = (f_0, f_1, \ldots, f_{N+1})$. The variable L maps the domain in which the $N+2$ points of x are allocated. Each term in F is defined through the operator:

$$f_n = \frac{\psi_{n+1} - 2\psi_n + \psi_{n-1}}{(\Delta x)^2} - \psi_n + 2\left|\psi_n\right|^2\psi_n + i\gamma\psi_n + h, \tag{8}$$

for $n = 1 \ldots N$ and at the boundaries by

$$f_0 = \frac{-3\psi_0 + 4\psi_1 - \psi_2}{2\Delta X}, \; f_{N+1} = \frac{\psi_{N-1} - 4\psi_N + 3\psi_{N+1}}{2\Delta X}. \tag{9}$$

The process of numerically search solutions involves iterating the expression:

$$\Psi^{(k+1)} = \Psi^{(k)} - p^k \left(\frac{\partial F}{\partial \Psi} \right)^{-1}_{\psi=\psi^k} F\left(\Psi^k\right), for \; k = 1, 2, \ldots \tag{10}$$

until, for a given iteration k, an error criterion is adopted based on the numerical tolerance. In the present study, such criterion is defined as:

$$\delta^{(k)} = \max_{0 \leq n \leq (N+1)} \left\{ \left| F\left(\Psi^{(k)}\right) \right| \right\} < tolerance. \tag{11}$$

The step p is responsible for decreasing the error at each iteration.

The initial point of the numerical search ($\Psi^{(0)}$) comes from the non-damped solutions, since analytical forms are known. For a given h, the damped numerical solutions are obtained for small increments in γ, so that a numerical continuation is followed. Similarly, taking as a starting point for the iteration a particular numerical solution obtained from a h x γ pair, a solution with a nearby h can be obtained.

3.2. Existence/stability diagram

By utilizing the methodology described in Section 3.1, it is possible to generate a diagram which delineates the regions where stationary solitonic solutions of Equation (3) exist. The boundaries of the existence and stability of solitons were elucidated in [13], where analytical and numerical limits were mapped. In parallel to the limits of existence, the Hopf bifurcation, which maps the area of temporal instability, was also identified.

Obtaining the Hopf bifurcation is of fundamental interest for chaotic systems [31], as this curve segregates regions of temporal instability despite the numerical convergence of Equation (4). There are studies in the field of nonlinear dynamics that use experimental data to obtain this curve [32], indicating a possible direction for validating the numerically achieved one.

As an approximation, the Hopf bifurcation curve is determined using a polynomial function (obtained through the least squares method) following the results outlined in [13]. The outcomes are summarized in Fig. 2, including the mathematical expressions used for the creation of the diagram.

According to [13], the approximation for the black curve (Fig. 2) is highly effective in delimiting the existence boundary of solutions. Other solitonic configurations (Table 1) exhibit distinct diagrams of existence and stability, as well as different shapes of stable solutions [33].

It is evident that the introduction of damping in the solitonic equation significantly reduces the range of h x γ pairs that enable the existence of solitons. As previously mentioned, this issue is of particular importance for mechanical systems, once damping cannot be usually neglected, and in numerous engineering applications, it is, in fact, a design variable.

4. Build of the metamodel

The construction of the metamodel is divided into two distinct and sequential stages. The first stage involves the creation of the Dataset that will be used in the second stage, the training of the neural network.

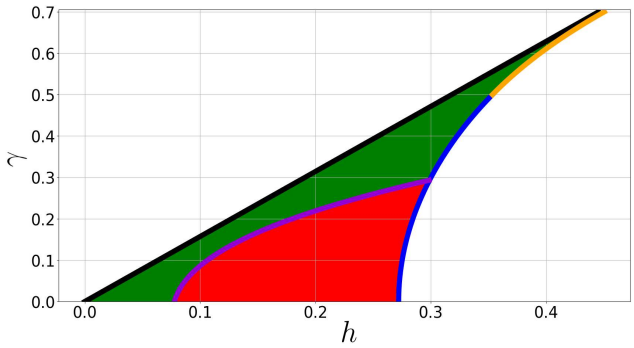

Figure 2: Existence and temporal stability diagram of solutions for Equation (4). Based on [13]. Black curve: $h - \frac{2\gamma}{\pi} = 0$. Blue curve: $h - \left(\frac{1}{3}\left(\frac{1}{3}\left(-\gamma^2 + \frac{1}{3}\right)^3\right)^{0.5} + \frac{1}{3}\left(\gamma^2 + \frac{1}{9}\right)\right)^{0.5} = 0$. Orange curve: $h - \left(\gamma^3 - \gamma^2 + \frac{\gamma}{2}\right)^{0.5} = 0$. Purple curve (Hopf bifurcation) : $h - (1.8728\gamma^3 + 1.6822\gamma^2 + 0.0997\gamma + 0.0777) = 0$. Regions of parameter $\gamma x h$ indicating the presence of stable solutions are depicted by the green area, while the red area illustrates the regions where unstable solutions occur.

4.1. Construction of the Dataset

From a computational standpoint, the generation of the Dataset is a costly process that requires an algorithm that balances processing time and approximation refinement. Despite the attempt to compare the performance of different Dataset sizes in various problems , the number of solutions required for efficient neural network training remains an open question in computer science [35, 36].

Section 3.1 introduced the numerical search strategy for solutions of Equation (4). The convergence of the method for $p^k = 1$, given a sufficiently close initial Ψ to the desired solution, has been proven [37]. Despite the guaranteed convergence, the practical feasibility of the method may be compromised in certain regions of the graph, specifically for high values of γ or low values

of h, the practical application of the Newton method considering $p^k = 1$ is inefficient. Hence, in order to increase the convergence speed of the method, a strategic step must be considered [38]. In this paper, this step will be determined by the relationship:

$$p^k = \max\left\{0.05, \frac{\delta^{(k-1)}}{\delta^{(k-1)} + \delta^{(k+1)}_{for:p^k=1}}\right\}. \tag{12}$$

As mentioned earlier, a numerical continuation for nearby solutions must be done. A solution will be considered near to another if and only if the γ values of each solution are distant by $\Delta\gamma$ or the h values of each solution are distant by Δh (not both at the same time). This consideration means that the iteration for the solution $\Psi(\gamma + \Delta\gamma, h)$ will start from $\Psi(\gamma, h)$, or, analogously, the solution $\Psi(\gamma, h + \Delta h)$ will also start from $\Psi(\gamma, h)$.

Based on non-damped solutions (Equation (5)), nearby solutions are constructed by exploring the possible parameter regions in a path (see Fig. 3a). In case of eventual divergences in the numerical search, the steps $\Delta\gamma$ and Δh are reduced in order to refine the numerical continuation. In the iterative implementation of nearby solutions, four numeric search stopping criteria are controlled (see Fig. 3b).

The criteria I, II, and III are chained, meaning that Criterion III only occurs after the verification of Criterion II, which, analogously, only occurs after the verification of Criterion I. If Criterion III or Criterion IV are reached, the solutions obtained on that numerical continuation path are stored, and a new path is constructed from a new non-damped solution. The simulation parameters are summarized in Table 2.

The choice of discretizing the simulation domain into $(N + 2)$ points

Table 2: Simulation parameters used in the creation of the Dataset

Parameter	Value
$\Delta\gamma$	$5\ 10^{-3}$
Δh	$5\ 10^{-10}$
Criterion I	10^2
Criterion II	$2\ 10^3$
Criterion III (h)	$5\ 10^{-4}$
Criterion III (γ)	$5\ 10^{-4}$
Tolerance	10^{-10}
Simulation domain of $[-L/2\ ,\ L/2]$	$[-50, +50]$
Number of points in the discretization of x	$6\ 10^2$
Number of paths	186
Number of obtained solutions (N_S)	27674

results in $2(N+2)$ values related to ψ ($(N+2)$ real components and $(N+2)$ imaginary components). Given these conditions, refined discretizations could considerably increase the computational time. The discretization also has an influence on non-damped solutions. Although these were obtained analytically, the discretization leads to numerical errors that propagate along the numerical continuation. Thus, before the search for damped solutions, it is recommended to use the Newton method in the non-damped solution in order to calibrate it according to the numerical tolerance.

Figure 3b summarizes the Dataset used in training the metamodel. As expected, except for regions of low h or high damping, the point solutions covers the entirety of the feasible region. The analytical superior boundary (Fig. 2, curve in black) is less covered by solutions if compared to the inferior numerical boundary (Fig.2, curves in blue and orange). The resultant number data points is 27674, which is in line with the order of magnitude of similar problems [39].

4.2. Neural network training strategy

The versatility and representational power of Feedforward Neural Networks (FNNs), aided by the ability of hidden neurons to extract higher-order statistics, enable their widespread application in various problem domains requiring predictive modeling from input data [14].

Using the python modules built by [34], an hyperparameter tuning is performed using the Bayesian Optimization to iteratively define the best configuration of the neural network. In this context, structural hyperparameters such as the number of hidden layers, the number of units within each layer, and the dropout percentage of each layer were taken into account. Ad-

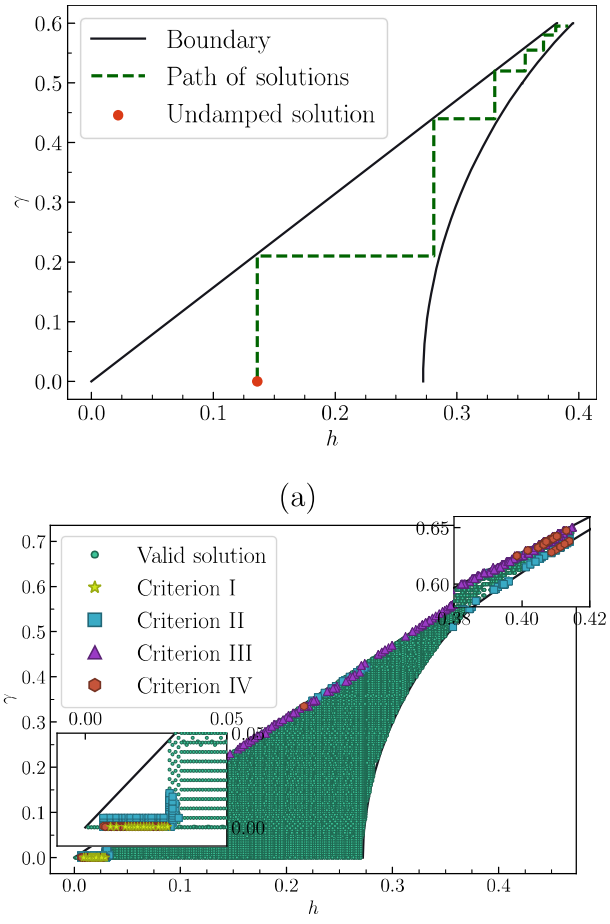

Figure 3: Example of the path followed by the numerical continuation from an undamped solution (a), and Dataset used in the construction of the neural network (b). The numeric search stopping criteria are I, related to the solution tolerance (Equation (11)); II, related to the maximum number of iterations required for convergence; III, related to the smallest value of steps $\Delta\gamma$ and Δh; and IV, related to the achievement of flat solutions.

ditionally, optimizer hyperparameters, such as the optimizer algorithm, the activation function, and the L2 regularization penalty, were also considered.

The final neural network configuration is shown in Fig. 4.

The data propagates from input layer $\Theta = [\gamma, h]$ to output layer $\mathbf{y} = [y_1, ..., y_{1200}]$ by the middle layer $\mathbf{S} = [S_1, ..., S_{200}]$. Two weight matrices are considered: $\mathbf{W_1}$ between the input and the intermediate layer and $\mathbf{W_2}$ between the layer and the output. Its definitions are made as follows:

$$\mathbf{W_{1(2x200)}} = \begin{bmatrix} P_{\gamma 1} & P_{\gamma 2} & ... & P_{\gamma 200} \\ P_{h1} & P_{h2} & ... & P_{h200} \end{bmatrix}, \tag{13}$$

$$\mathbf{W_{2(200x1200)}} = \begin{bmatrix} P_{y_1 1} & P_{y_2 1} & ... & P_{y_{1200} 1} \\ P_{y_1 2} & P_{y_2 2} & ... & P_{y_{1200} 2} \\ \vdots & \vdots & \vdots & \vdots \\ P_{y_1 200} & P_{y_2 200} & ... & P_{y_{1200} 200} \end{bmatrix}. \tag{14}$$

The relationship between the elements that form the layers is expressed by two constitutive equations. The first one corresponds to the relation between the input and the intermediate layer:

$$S_i = \Theta \cdot \mathbf{W_{1i}}, \tag{15}$$

where $\mathbf{W_{1i}}$ is the vector formed by the elements of column i of $\mathbf{W_1}$. The hidden layer is fed through an activation function φ, which consists of a Rectified Linear Unit (ReLU), and computes $\hat{\mathbf{S}}$. The second constitutive equation is between the intermediate layer and the output:

$$y_i = \hat{\mathbf{S}} \cdot \mathbf{W_{2i}} + b, \tag{16}$$

where $\mathbf{W_{2i}}$ is the vector formed by the elements of column i of $\mathbf{W_2}$.

The parameters $\mathbf{W_1}$, $\mathbf{W_2}$ and b are updated with automatic differentiation and back propagation method, until the chosen loss is satisfactory [16]. In the present work, the loss function used to train the network is the Mean Square Error (MSE) with L2 regularization:

$$MSE = \frac{1}{1200}\sum_{i=1}^{1200}(y_i - \hat{y}_i)^2 + \lambda\sum_{j=1}^{P}|\mathbf{W}_j|^2 . \tag{17}$$

where λ is the regularization rate equal to 0.001 and P is the total number of weights in the model. The first 600 values of $\mathbf{y}$ are the real prediction values, while the last 600 values are imaginary.

Before the model training, the data is randomly separated into train and test subsets, with 80/20 percent ratio, followed by a standardization of the input data. This standardization is obtained by identifying the mean of γ and h, respectively

$$\mu_\gamma = \tfrac{1}{N_S}\textstyle\sum_{i=1}^{N_S}\gamma_i \quad \text{and} \quad \mu_h = \tfrac{1}{N_S}\textstyle\sum_{i=1}^{N_S} h_i$$

and applying the following transformation on the values:

$$\hat{\gamma}_k = \tfrac{\gamma_k - \mu_\gamma}{\sigma_\gamma} \quad \text{and} \quad \hat{h}_k = \tfrac{h_k - \mu_h}{\sigma_h},$$

where

$$\sigma_\gamma = \sqrt{\tfrac{\sum_{i=1}^{N_S}(\gamma_i - \bar{\mu}_\gamma)^2}{N_S}} \quad \text{and} \quad \sigma_h = \sqrt{\tfrac{\sum_{i=1}^{N_S}(h_i - \bar{\mu}_h)^2}{N_S}} \ .$$

The maximum number of epochs is 500 with a early stopping training criteria that monitors the loss decrease. This criterion plays the role of avoiding unnecessary computational costs and overfitting, where, after identifying the epoch at which the decrease in the value of the loss no longer occurs, the training is interrupted for the next 50 epochs.

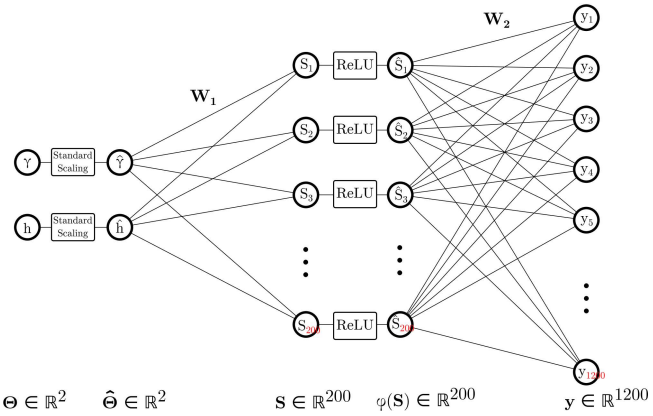

Figure 4: Architecture of the neural network obtained by the hyperparameter analysis.

5. Predictive ability and computational gain of the metamodel

The numerical convergence of possible solutions of Equation (4) requires increasingly finer refinements as the simulation approaches the solitonic existence boundary. As highlighted in Section 4.1, this consideration becomes particularly evident when high values of γ are chosen: the choice of parameters from Table 2 allowed the identification of damped solitons up to $\gamma \approx 0.65$. Another region of difficult convergence is found at low values of the variable h (Fig. 3b). This numerical characteristic points to a possible difficulty in stabilizing localized vibrating modes in chains of oscillators whose balance between nonlinearity and excitation is not achieved in such a way as to overcome damping [25]. As can be observed on Fig. 5a, the prediction/extrapolation made by the metamodel carries this feature.

After creating the metamodel, an investigation regarding the accuracy area is recommended. Despite training the Neural Network through Equation (17) for the entire x domain, the largest values of $|\psi|$ are centered around 0

(Fig. 5b). From the perspective of the ILM in oscillator chains, errors related to points of higher amplitudes are more relevant than errors linked to points approaching the boundaries. Under this perspective, an error criterion that weighs location can be proposed by considering Equation (17) in a domain near the origin. In this article, the error analysis domain is limited to $0.25 \leq x \leq 0.25$ (Fig. 5b).

Figure 6a delimits a region where, after analyzing errors concentrated at the origin, only predictions with errors less than 1% of the maximum error are accepted. As can be seen again, a similar conclusion obtained by the Newton method can be obtained by observing the metamodel's performance area: regions with high values of γ or low values of h impair the metamodel's predictive ability. As can be verified from Fig. 6b, using the metamodel in remote regions of the boundary leads to progressively closer approximations to the solutions obtained by Newton's method.

Figure 7 presents a graph illustrating the relationship between the computational time required to obtain solutions for Equation (4), varying the parameter gamma (using the same parameters as Table 2). It was observed that the processing time quickly reaches an order of magnitude hours. On average, the processing time of the metamodel for the simulated $hx\gamma$ pairs was 53 ms, with a maximum time of 71 ms and a minimum of 50 ms. The simulations were performed on a Dell Precision T1700 Tower with an Intel Xeon processor, model E3-1220 v3, featuring 4 cores and a base frequency of 3.10 GHz, 8 GB of RAM, an NVIDIA Quadro K600 graphics card, and Ubuntu 22.04 operating system.

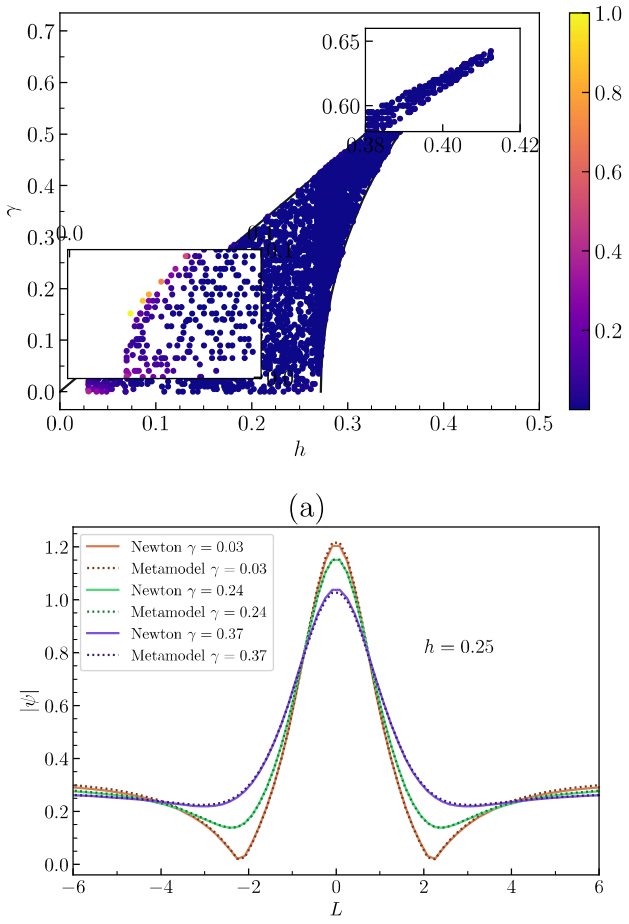

(a)

(b)

Figure 5: Normalized prediction errors of the metamodel by the maximum MSE obtained (a) and graphical comparison between the $|\psi|$ calculated using the metamodel and the Newton method.

6. Conclusion and future directions

In summary, this paper presents a metamodel based on artificial neural networks for stationary solitons in nonlinear oscillator chains subjected to external excitation. The metamodel is effective in describing the solitonic

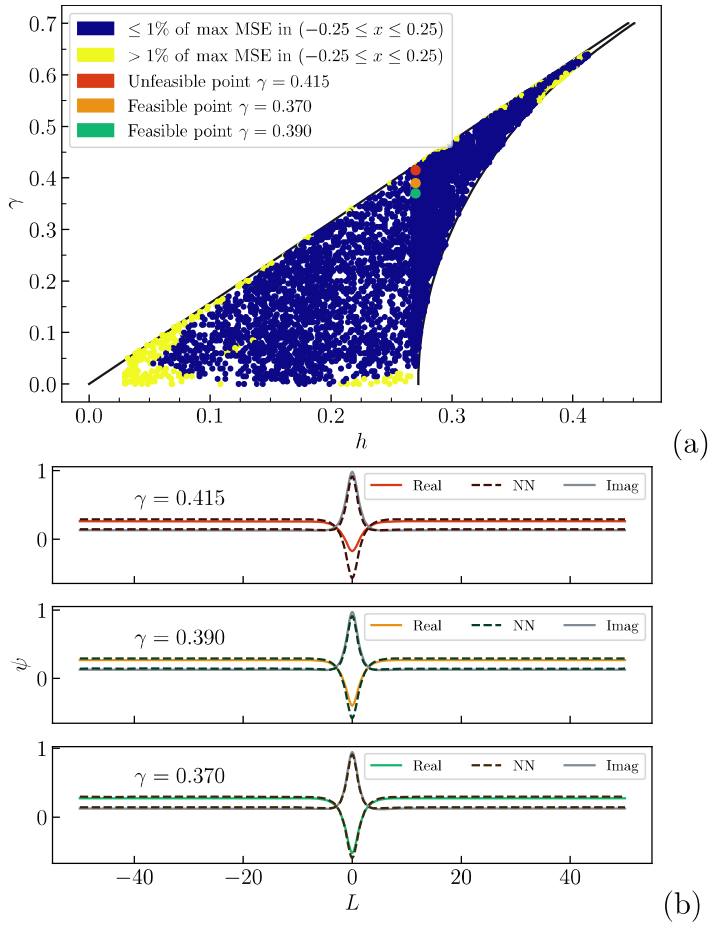

Figure 6: Area of best performance of the metamodel based on controlling MSE centered at the origin (a) and comparison of solitons obtained by the Newton method and the metamodel as the parameters approach the boundary.

behavior of the NLSE within a region of parameters numerically verified by Newton's method.

This study is driven by the localized vibrations in coupled resonators, particularly in damped structures, where, considering only external excitation, analytical solutions are not reported. Although the main motivation

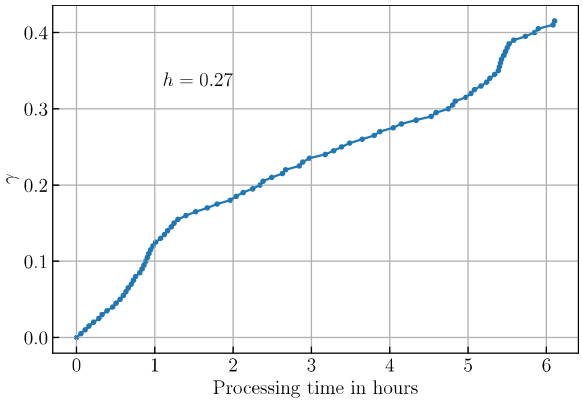

Figure 7: Relationship between processing times and solitonic solutions obtained by the Newton method.

of this work has its origin in vibration dynamics, it is expected that the results presented here will contribute to the development of new applications in several fields, such as optics or metamaterials, where the NLSE plays a fundamental role in describing physical phenomena.

The Dataset used for training the network can be found in [40] so that other strategies for obtaining a metamodel can be implemented by other researchers, either through the use of metamodels as a function of the region of the parameters or of new architecture proposals.

Future directions include the extension of the methodology to other types of nonlinear damped systems where closed solutions are unknown and computationally expensive.

Declaration of competing interest

The authors declare that they have no known competing financial interests or personal relationships that could have appeared to influence the work

reported in this paper.

Acknowledgments

We gratefully acknowledge support from EUR EIPHI program, Europe (Contract No. ANR 17-EURE-0002). This work was also performed in cooperation with the Coordenaçào de Aperfeiçoamento de Pessoal de Nível Superior - Brasil (CAPES) – Finance Code 88887.696945/2022-00.

References

[1] Kenig, E., Malomed, B. A., Cross, M. C., Lifshitz, R. (2009). Intrinsic localized modes in parametrically driven arrays of nonlinear resonators. Physical Review E, 80(4), 046202.

[2] El-Tantawy, S. A., Salas, A. H., Alyousef, H. A., Alharthi, M. R. (2022). Novel approximations to a nonplanar nonlinear Schrödinger equation and modeling nonplanar rogue waves/breathers in a complex plasma. Chaos, Solitons Fractals, 163, 112612.

[3] Boopathy, C., Kavitha, L., Ravichandran, R. (2022). Nonlinear modelling of soliton collision dynamics for blood flow in a stenotic artery. Materials Today: Proceedings, 51, A1-A13.

[4] Shehzad, K., Seadawy, A. R., Wang, J., Arshad, M. (2023). Multi peak solitons and btreather types wave solutions of unstable NLSEs with stability and applications in optics. Optical and Quantum Electronics, 55(1), 7.

[5] Hernández, S. M., Bonetti, J., Linale, N., Grosz, D. F., Fierens, P. I. (2022). Soliton solutions and self-steepening in the photon-conserving nonlinear Schrödinger equation. Waves in Random and Complex Media, 32(5), 2533-2549.

[6] Ali, A. S., Govindarajan, A., Lakshmanan, M. (2022). Filamentation and stabilization of vortex solitons in nonlinear metamaterial waveguides. Physics Letters A, 451, 128416.

[7] Bitar, D. (2017). Collective dynamics of weakly coupled nonlinear periodic structures (Doctoral dissertation, Université Bourgogne Franche-Comté).

[8] Manav, M., Phani, A. S., Cretu, E. (2018). Mode localization and sensitivity in weakly coupled resonators. IEEE Sensors Journal, 19(8), 2999-3007.

[9] Spletzer, M., Raman, A., Sumali, H., Sullivan, J. P. (2008). Highly sensitive mass detection and identification using vibration localization in coupled microcantilever arrays. Applied Physics Letters, 92(11), 114102.

[10] Brazhnyi, V. A., Jisha, C. P., Rodrigues, A. S. (2013). Interaction of discrete nonlinear Schrödinger solitons with a linear lattice impurity. Physical Review A, 87(1), 013609.

[11] Adilkhanov, A. N., Taimanov, I. A. (2017). On numerical study of the discrete spectrum of a two-dimensional Schrödinger operator with soliton potential. Communications in Nonlinear Science and Numerical Simulation, 42, 83-92.

[12] Farag, N. G., Eltanboly, A. H., El-Azab, M. S., Obayya, S. S. A. (2021). On the analytical and numerical solutions of the one-dimensional nonlinear Schrodinger equation. Mathematical Problems in Engineering, 2021, 1-15.

[13] Barashenkov, I. V., Smirnov, Y. S. (1996). Existence and stability chart for the ac-driven, damped nonlinear Schrödinger solitons. Physical Review E, 54(5), 5707.

[14] Shirvany, Y., Hayati, M., Moradian, R. (2008). Numerical solution of the nonlinear Schrodinger equation by feedforward neural networks. Communications in Nonlinear Science and Numerical Simulation, 13(10), 2132-2145.

[15] Li, J., Chen, Y. (2020). A deep learning method for solving third-order nonlinear evolution equations. Communications in Theoretical Physics, 72(11), 115003.

[16] Wang, R. Q., Ling, L., Zeng, D., Feng, B. F. (2021). A deep learning improved numerical method for the simulation of rogue waves of nonlinear Schrödinger equation. Communications in Nonlinear Science and Numerical Simulation, 101, 105896.

[17] Liu, Z., Madhavan, V., Tegmark, M. (2022). Machine learning conservation laws from differential equations. Physical Review E, 106(4), 045307.

[18] Wu, G. Z., Fang, Y., Wang, Y. Y., Wu, G. C., Dai, C. Q. (2021). Predicting the dynamic process and model parameters of the vector

optical solitons in birefringent fibers via the modified PINN. Chaos, Solitons Fractals, 152, 111393.

[19] Pu, J., Li, J., Chen, Y. (2021). Solving localized wave solutions of the derivative nonlinear Schrödinger equation using an improved PINN method. Nonlinear Dynamics, 105, 1723-1739.

[20] Niedergesäß, B., Papangelo, A., Grolet, A., Vizzaccaro, A., Fontanela, F., Salles, L., ... Hoffmann, N. (2021). Experimental observations of nonlinear vibration localization in a cyclic chain of weakly coupled nonlinear oscillators. Journal of Sound and Vibration, 497, 115952.

[21] Fontanela, F., Grolet, A., Salles, L., Chabchoub, A., Hoffmann, N. (2018). Dark solitons, modulation instability and breathers in a chain of weakly nonlinear oscillators with cyclic symmetry. Journal of Sound and Vibration, 413, 467-481.

[22] Kimura, M., Hikihara, T. (2012). Experimental manipulation of intrinsic localized modes in macro-mechanical system. Nonlinear Theory and Its Applications, IEICE, 3(2), 233-245.

[23] Lee, S., Kato, M., Doi, Y., Hirata, K. (2021). A New Method to Control Intrinsic Localized Mode Using a Variable Magnetic Spring Structure. IEEE Transactions on Magnetics, 58(2), 1-5.

[24] Grolet, A., Hoffmann, N., Thouverez, F., Schwingshackl, C. (2016). Travelling and standing envelope solitons in discrete non-linear cyclic structures. Mechanical systems and signal processing, 81, 75-87.

[25] Jallouli, A., Kacem, N., Bouhaddi, N. (2017). Stabilization of solitons in coupled nonlinear pendulums with simultaneous external and parametric excitations. Communications in Nonlinear Science and Numerical Simulation, 42, 1-11.

[26] Fontanela, F., Grolet, A., Salles, L., Chabchoub, A., Champneys, A. R., Patsias, S., Hoffmann, N. (2019). Dissipative solitons in forced cyclic and symmetric structures. Mechanical Systems and Signal Processing, 117, 280-292.

[27] Adile, A. D., Kenmogne, F., Tewa, A. K. S., Simo, H., Tahir, A. M., Kumar, S. (2021). Dynamics of a mechanical network consisting of discontinuous coupled system oscillators with strong irrational nonlinearities: resonant states and bursting waves. International Journal of Non-Linear Mechanics, 137, 103812.

[28] Balachandran, B., Magrab, E. B. (2018). Vibrations. Cambridge University Press.

[29] Djine, A., Deffo, G. R., Yamgoué, S. B. (2023). Bifurcation of backward and forward solitary waves in helicoidal Peyrard–Bishop–Dauxois model of DNA. Chaos, Solitons Fractals, 170, 113334.

[30] Barashenkov, I. V., Zemlyanaya, E. V. (2011). Travelling solitons in the externally driven nonlinear Schrödinger equation. Journal of Physics A: Mathematical and Theoretical, 44(46), 465211.

[31] Yao, K. E., Shi, Y. (2019). Hopf bifurcation in three-dimensional based on chaos entanglement function. Chaos, Solitons Fractals: X, 4, 100027.

[32] Jiménez–Ramírez, O., Cruz–Domínguez, E. J., Quiroz–Juárez, M. A., Aragón, J. L., Vázquez–Medina, R. (2021). Experimental detection of hopf bifurcation in two-dimensional dynamical systems. Chaos, Solitons Fractals: X, 6, 100058.

[33] Barashenkov, I. V., Bogdan, M. M., Korobov, V. I. (1991). Stability diagram of the phase-locked solitons in the parametrically driven, damped nonlinear Schrödinger equation. Europhysics Letters, 15(2), 113.

[34] O'Malley, T., Bursztein, E., Long, J., Chollet, F., Jin, H., Invernizzi, L., Others. (2019). KerasTuner. Retrieved from https://github.com/keras-team/keras-tuner

[35] Catal, C., Diri, B. (2009). Investigating the effect of dataset size, metrics sets, and feature selection techniques on software fault prediction problem. Information Sciences, 179(8), 1040-1058.

[36] Hou, A., Jin, S., Harmuth, H., Gruber, D. (2019). Thermal and thermomechanical responses prediction of a steel ladle using a back-propagation artificial neural network combining multiple orthogonal arrays. steel research international, 90(7), 1900116.

[37] Gavurin, M. K. (1958). Nonlinear functional equations and continuous analogues of iteration methods. Izvestiya Vysshikh Uchebnykh Zavedenii. Matematika, (5), 18-31.

[38] Ermakov, V. V., Kalitkin, N. N. (1981). The optimal step and regularization for Newton's method. Zhurnal Vychislitel'noi Matematiki i Matematicheskoi Fiziki, 21(2), 491-497.

[39] Salmela, L., Tsipinakis, N., Foi, A., Billet, C., Dudley, J. M., Genty, G. (2021). Predicting ultrafast nonlinear dynamics in fibre optics with a recurrent neural network. Nature machine intelligence, 3(4), 344-354.

[40] SENA, J. P., BARBOSA, A. S., BOUHADDI, N., KACEM, N. (2023). Nonlinear Schrödinger Equation Dataset [Data set]. https://github.com/senajoaop/nlse-dataset

Declaration of interests

☒The authors declare that they have no known competing financial interests or personal relationships that could have appeared to influence the work reported in this paper.

☐The authors declare the following financial interests/personal relationships which may be considered as potential competing interests:

fig1

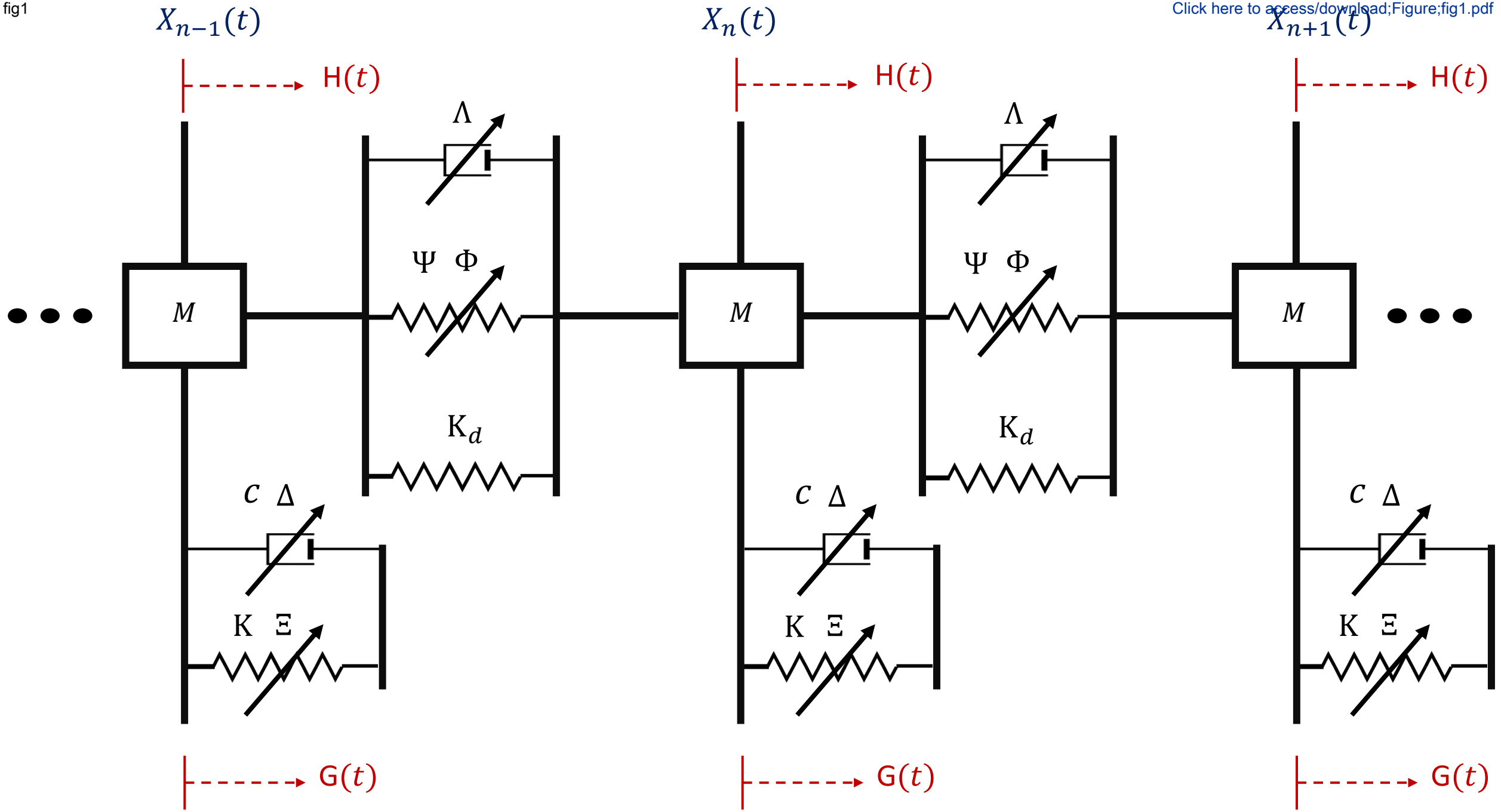

fig2

Click here to access/download;Figure;fig2.pdf

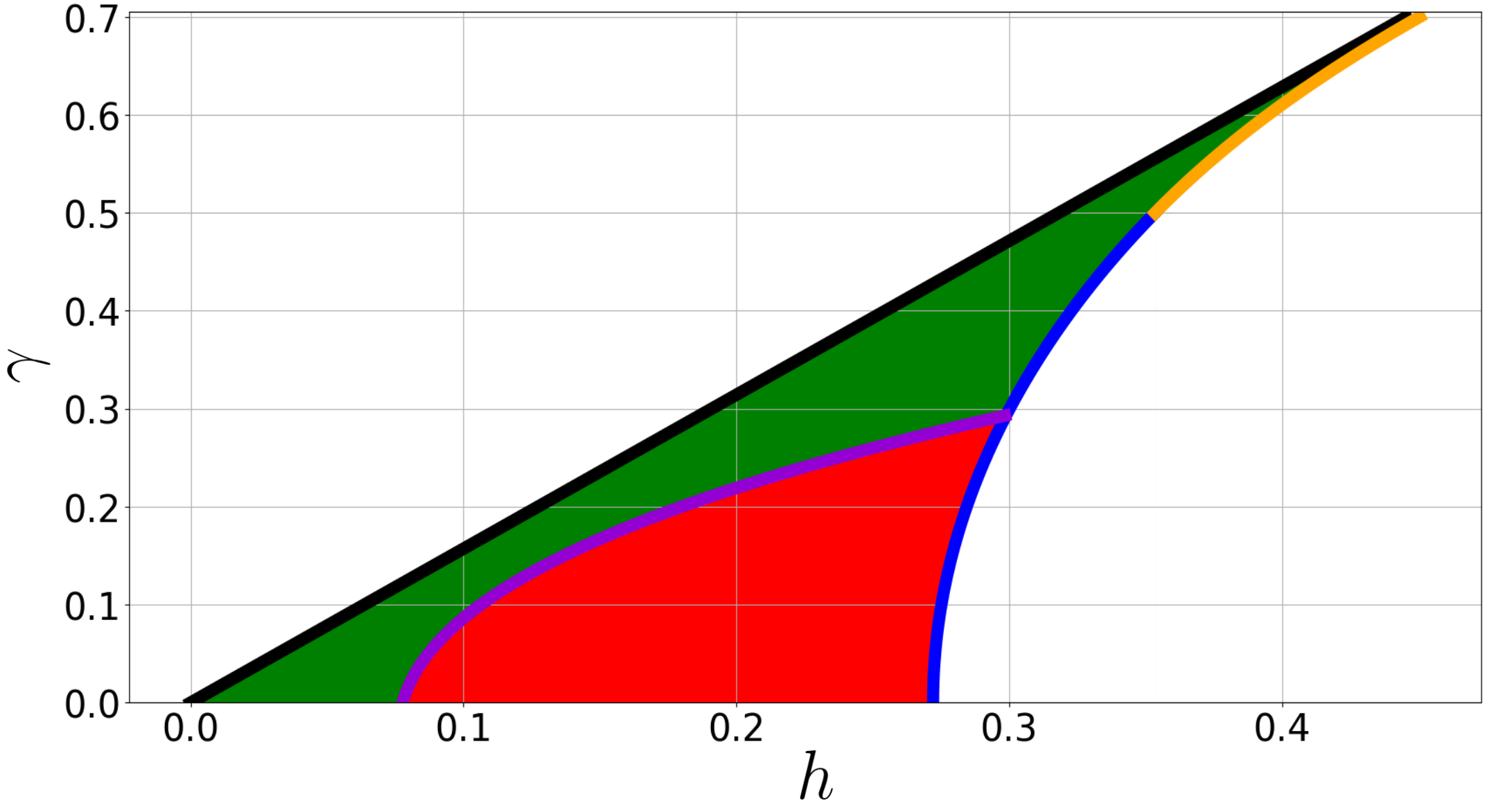

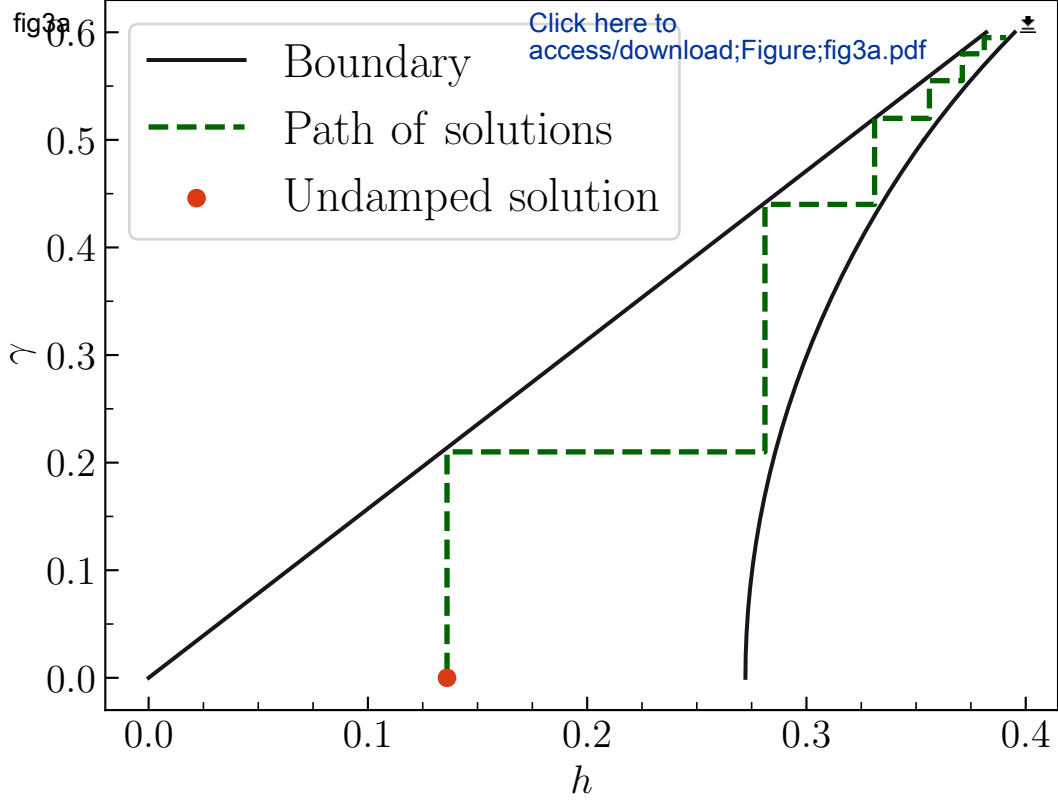
fig3a
Click here to
access/download;Figure;fig3a.pdf
Boundary
Path of solutions
Undamped solution
0.6
0.5
0.4
0.3
0.2
0.1
0.0
γ
0.0
0.1
0.2
0.3
0.4
h

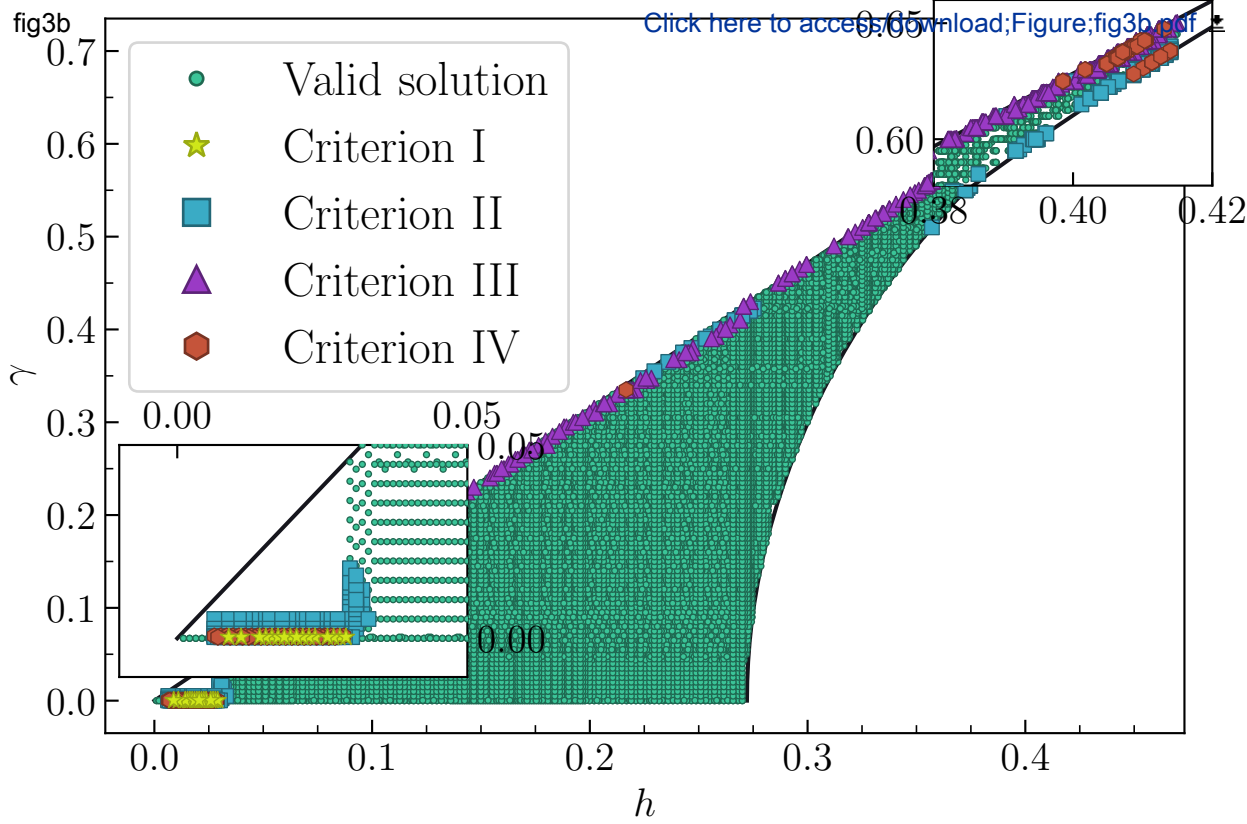

fig4

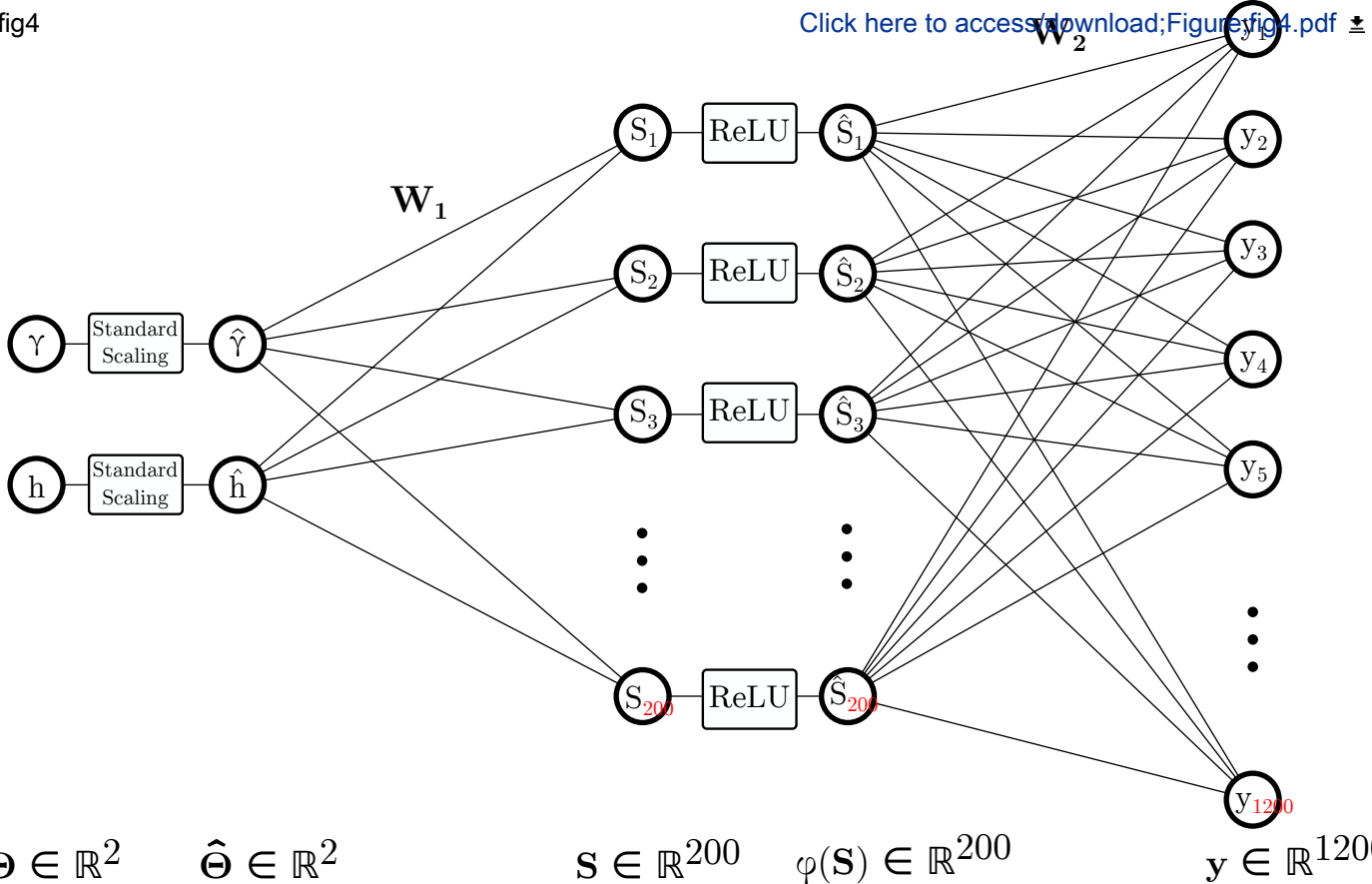

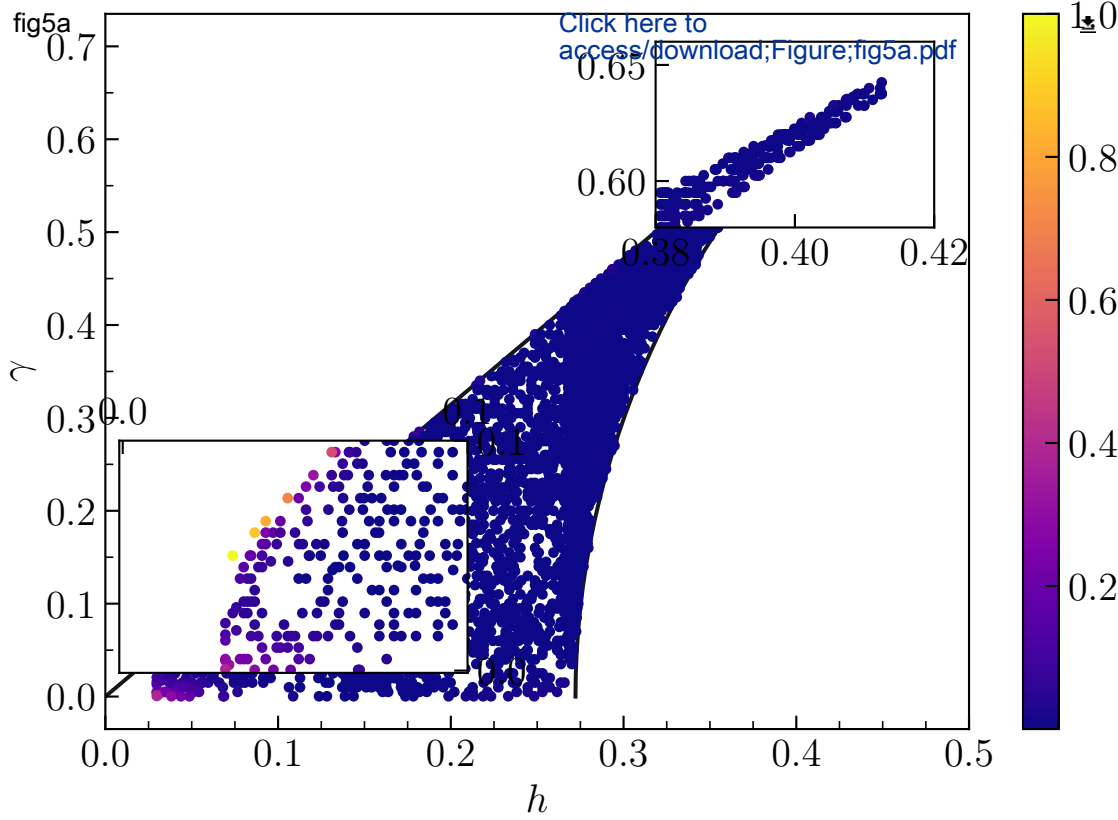
fig5a
Click here to
access/download;Figure;fig5a.pdf
0.7
0.6
0.5
0.4
0.3
0.2
0.1
0.0
γ
0.0
0.1
0.2
0.3
0.4
0.5
h
0.65
0.60
0.38
0.40
0.42
0.0
0.1
0.00
1.0
0.8
0.6
0.4
0.2

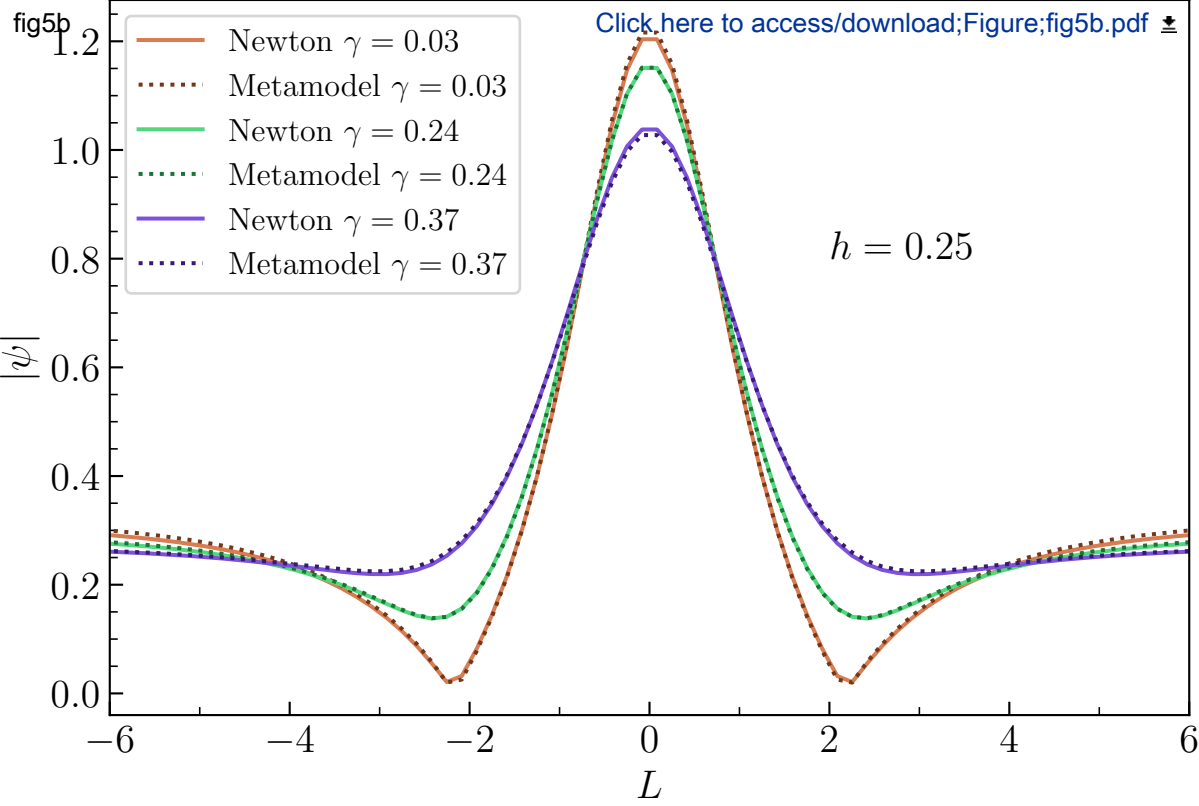
fig5b
Click here to access/download;Figure;fig5b.pdf
Newton $\gamma = 0.03$
Metamodel $\gamma = 0.03$
Newton $\gamma = 0.24$
Metamodel $\gamma = 0.24$
Newton $\gamma = 0.37$
Metamodel $\gamma = 0.37$
$h = 0.25$
$|\psi|$
L
0.0
0.2
0.4
0.6
0.8
1.0
1.2
−6
−4
−2
0
2
4
6

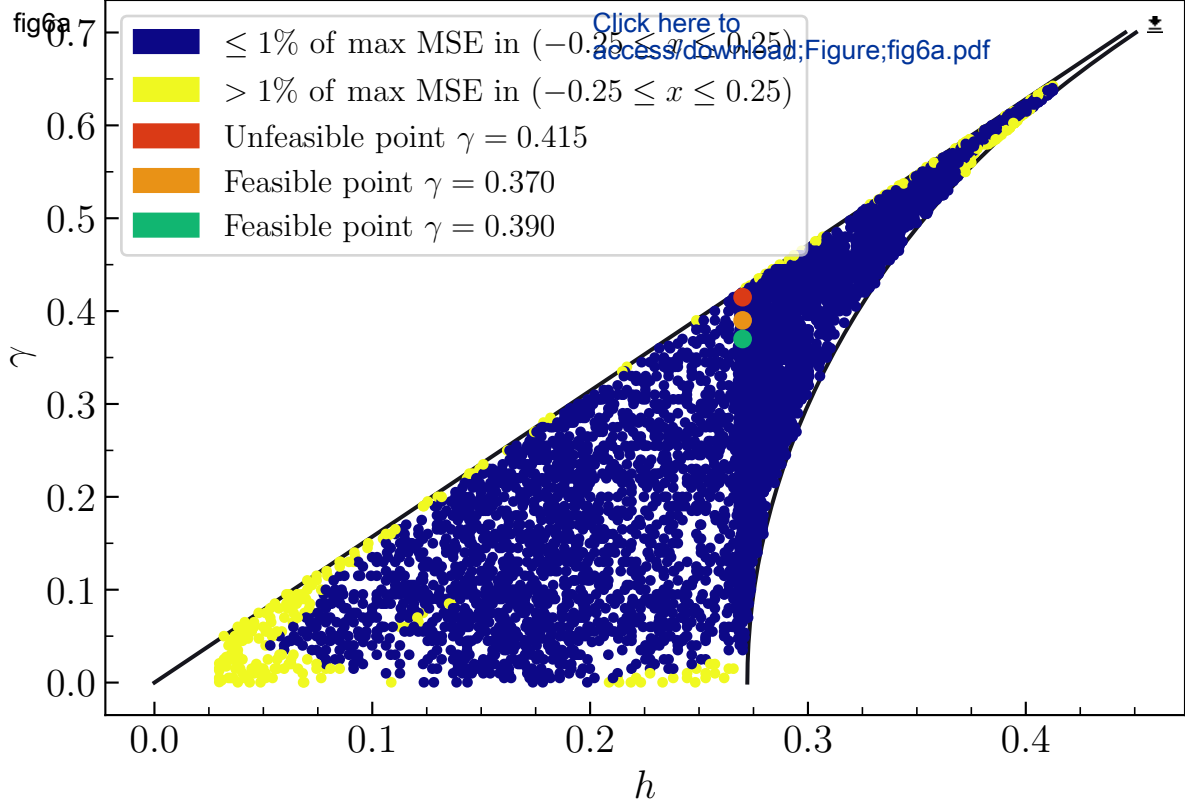
fig6a
Click here to access/download;Figure;fig6a.pdf
$\leq 1\%$ of max MSE in $(-0.25 \leq x \leq 0.25)$
$> 1\%$ of max MSE in $(-0.25 \leq x \leq 0.25)$
Unfeasible point $\gamma = 0.415$
Feasible point $\gamma = 0.370$
Feasible point $\gamma = 0.390$
γ
h
0.0
0.1
0.2
0.3
0.4
0.5
0.6
0.7